Supporting Information

Ambipolar Charge Distribution in Donor-Acceptor Polymer Field-effect Transistors

Xin Yu Chin,[a] Giuseppina Pace,*[b] Cesare Soci,[ac] and Mario Caironi*[b]

[a]Division of Physics and Applied Physics, School of Physical and Mathematical Sciences, Nanyang Technological University, 21 Nanyang Link, Singapore 637371.

[b]Center for Nano Science and Technology @PoliMi, Istituto Italiano di Tecnologia, Via G. Pascoli 70/3, 20133 Milano, Italy.

[c]Centre for Disruptive Photonic Technologies, Nanyang Technological University, 21 Nanyang Link, Singapore 637371.

Table S1. Work function measured on solvent rinsed, bare Au gold electrodes and on Au electrodes modified with different PEI and solvent treatements.

Sample	Work function (eV)
1- Au/PEI (0.1% methoxyethanol) annealing 100°, 10 min, post annealing rinsing with water (1 min), N_2 drying	4.17 ± 0.05
2- Au/PEI (0.1% methoxyethanol), rinsing with IPA (No Annealing), N_2 drying	4.23 ± 0.05
3- Bare Au, rinsing with IPA, N_2 drying	4.96 ± 0.05
4- Bare Au, rinsing with methoxyethanol, N_2 drying	4.75 ± 0.05

The work function was measured by means of a commercial set-up (Kelvin Probe from KP technology). Au was thermally evaporated on a mica substrate, on top of a Cr adhesion layer (as done also for the Au electrodes present in the devices reported in the main text).
The solution of branched polyethylenimine PEI 0.4% in methoxyethanol, was prepared as indicated in the main text and spin coated onto the substrates.
In 1- the same procedure used to modify the Au electrode of the FET with PEI was used for this Au substrate, consisting of spin coating the PEI solution onto the Au substrate, an annealing at 100 ºC for 10 min in ambient air, followed by the surface rinsing with a mild flow of distilled water for 1 minute and dried with nitrogen flow.

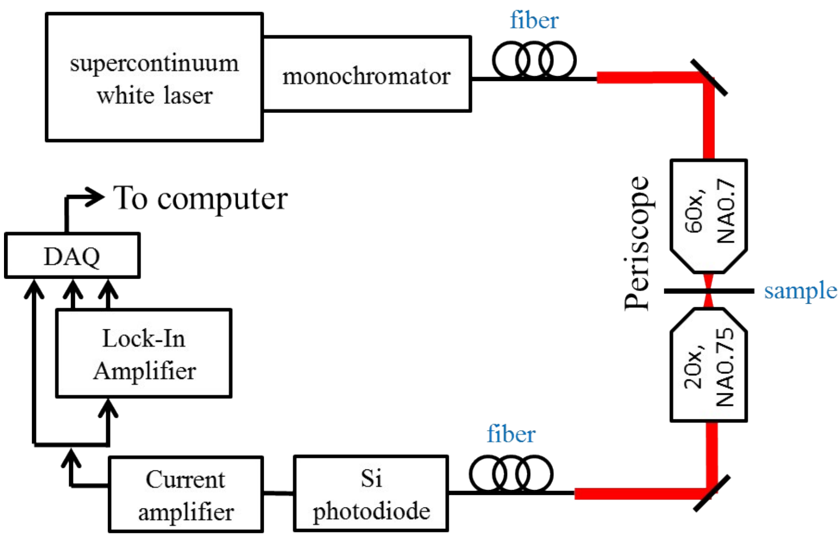

Figure S1. Charge modulation microscopy setup.

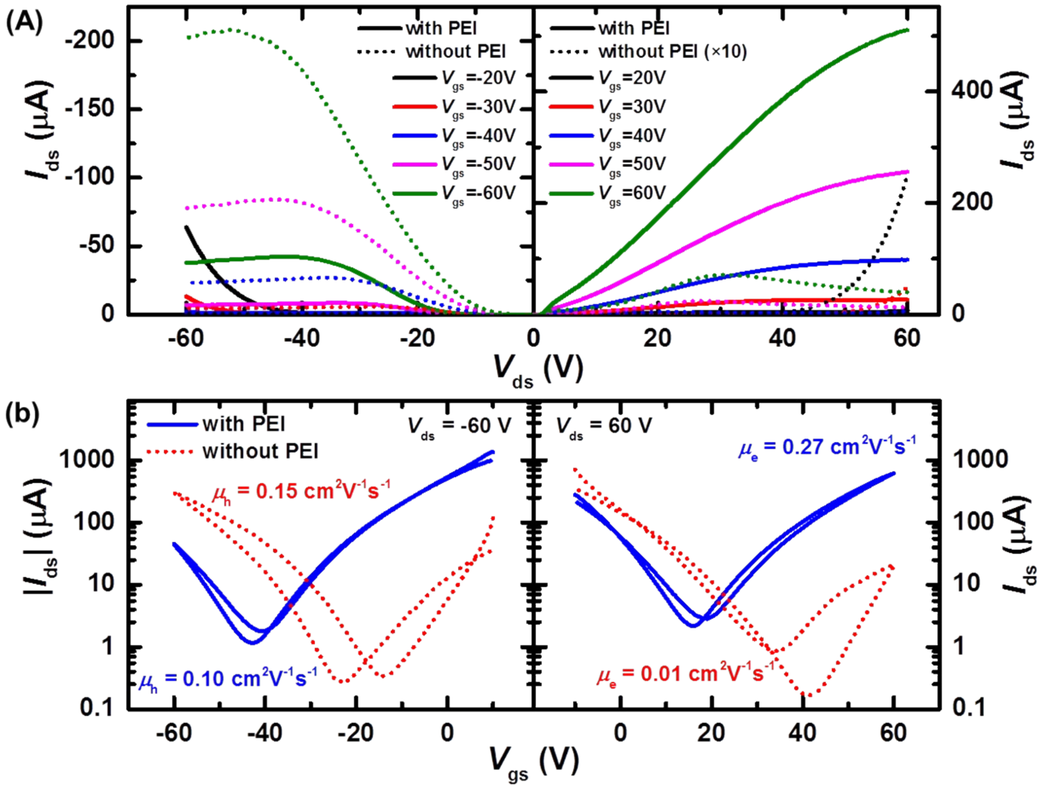

Figure S2. Comparison of DPPT-TT FETs with and without PEI layer. Output (a) and transfer (b) characteristics of the fabricated DPPT-TT FETs. The solid blue and dotted red curves represent the characteristics of devices fabricated with and without PEI layer, respectively.

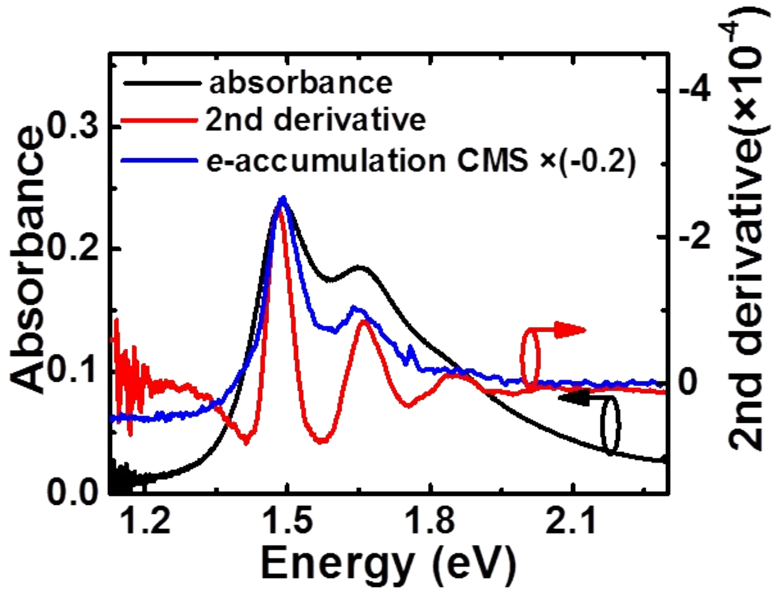

Figure S3. Optical properties of DPPT-TT. Absorbance (black) and second derivative (red) spectra of DPPT-TT thin film. CMS spectrum (blue, under electron accumulation V_{gs} = 40 V ± 20 V) collected at the channel center is also shown for comparison.

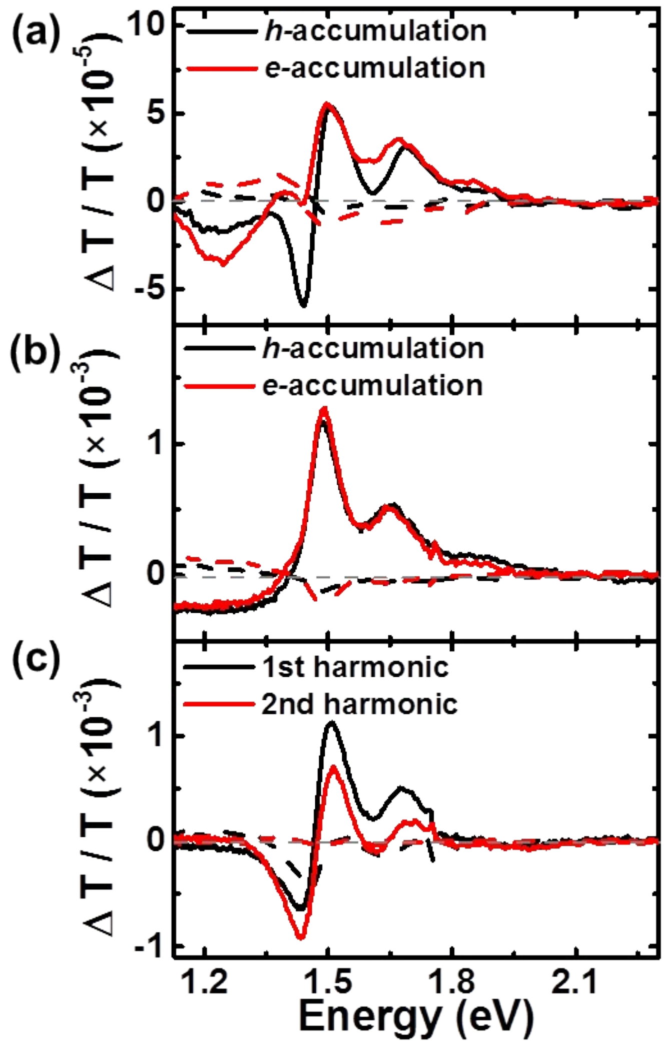

Figure S4 Optical characteristics of DPPT-TT. (a) Macroscopic CMS spectra for hole (black, V_{gs} = -40 V $\pm$ 10 V) and electron (red, V_{gs} = 40 V $\pm$ 10 V) accumulation regimes collected by probing the entire FET device. In-phase and quadrature phase signals are shown with continuous and dashed lines, respectively. The spectra are acquired with source and drain at ground (V_s = V_d = 0 V). (b) Local CMS spectra for *h*-accumulation (black) and *e*-accumulation (red) regimes acquired by probing at the FET channel center. (c) 1st harmonic (black) and 2nd harmonic (red) CMS spectra acquired at electrode edge. The spectra are acquired with V_{gs} = -40 V ± 20 V and V_{ds} = 0 V.

Fig. S4(a) shows CMS spectra collected by probing the entire FET, while Fig. S4(b) and Fig. S4(c) show CMS spectra acquired by locally probing at FET channel center and electrode edge, respectively. We observe a contribution of quadrature phase signal in the CMS especially for the 1st harmonic spectrum (as shown in Fig. S4(c)). The quadrature phase signal accounts for the presence of long lived species,[1] which do not have a linear response with respect to the gate modulation frequency.

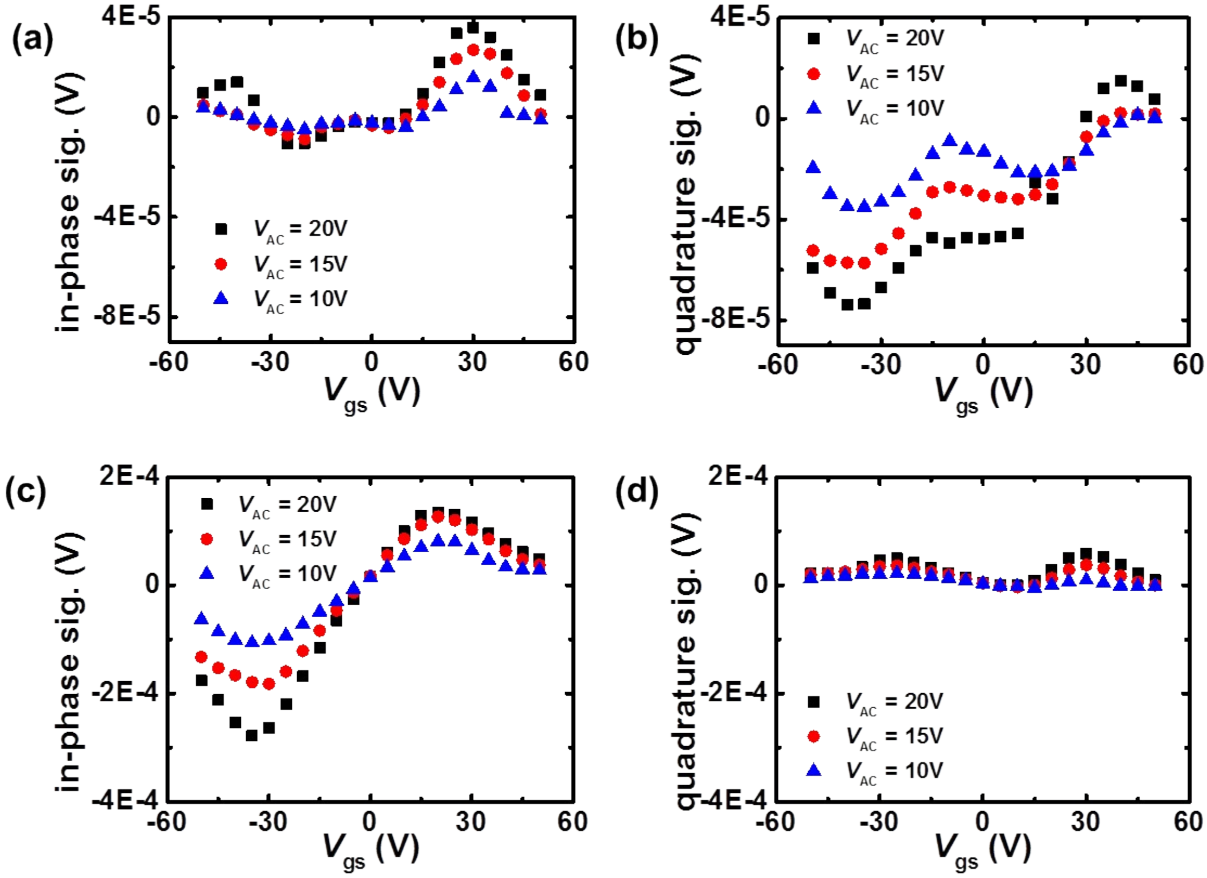

Figure S5. Voltage-modulation optical characteristics of DPPT-TT FET at the electrode edge. (a, b) In-phase (a) and quadrature phase (b) of electro-absorption (2nd harmonic) signal at probing wavelength of 1.49 eV. (c, d) In-phase (c) and quadrature phase (d) of charge-induced absorption (1st harmonic) signal at probing wavelength of 1.49 eV. All measurements were acquired at 50 KHz modulation frequency with drain and source electrodes are grounded.

Being highly sensitive to the electric field, the EA signal can be used as a tool to better elucidate the role of the contact resistance in device physics of FET. Contact resistance in FETs arises from the imperfect alignment between the semiconductor HOMO (or LUMO) level and work function of the injecting electrodes, hence resulting in the formation of an injection barrier and potential drop across the semiconductor-electrode interface which reduces the injection efficiency.[2] Here, we monitor the change in optical response at 1.49 eV in the 1ω and 2ω by probing at electrode edge with different gate biases (Fig. S5). It is worth to mention that charge-induced absorption/bleaching signals might also contribute to the 1ω signal since they both show AC electric field dependence,[3] while the 2ω component is solely originated only from EA signal. Note that Equation 1 below is a function of the electric field applied across the active channel of an operating device.

In Fig. S5(c), we can observe the monotonic dependence of the 1ω signal over the V_{gs} from -35 V to 20 V. The corresponding gate bias range in 2ω signal (Fig. S5(b)) reveals two minima at V_{gs} = 20 V and V_{gs} = -35 V. The monotonic 1 ω dependence is likely due to the superposing contribution of the bleaching characteristics from the buildup of the charge accumulation and the EA signal from polarization field as evidenced by the 2ω signal measurement. Beyond this range, *i.e.* V_{gs} > 20 V and V_{gs} < -35 V, the 2ω signal (Fig. S5(b)) is becoming less negative, indicating the EA signal contribution is decreasing. This is also evidenced by the drop and increasing 1ω signal Fig. S5(c) when V_{gs} > 20 V and V_{gs} < -35 V, respectively. This indicates that the EA signals are built-up by the accumulated and trapped carriers at the electrode due to the injection barrier and are significantly screened upon improvement of carrier injection as gate voltage increases beyond respective threshold voltage of holes and electron accumulation. This is also supported by the observation of signal minima in 2ω signal at V_{gs} = 20 V and V_{gs} = -35 V, which are roughly corresponding to the minima points ($V_{gs} \approx$ 20 V and $V_{gs} \approx$ -40 V) in FET transfer characteristic measurement at V_{ds} = 60 V and V_{ds} = -60 V (Fig. 1(c)), respectively. It is generally hard to define the threshold voltages for each carrier in an ambipolar FET since the FET is hardly turned off due its' capability to transport hole and electron effectively. In this case, the EA signal provides a good opportunity to study the injection of holes and electrons. The signal minima in 2ω signal at V_{gs} = 20 V and V_{gs} = -35 V could indicate the minimal voltage required for electron and hole, respectively, to overcome respective injection barrier.

However, we could still observe non-zero 2ω in-phase (Fig. S5(a)) and 1ω quadrature phase (Fig. S5(d)) signals despite measurements were performed at modulation frequency of 50 kHz (limited by lock-in amplifier). For FET, the internal electric field is not necessarily having a linear dependency on applied V_g and V_{ds}. In particular, bias induced charge trapping at the metal-semiconductor interface can introduce an interfacial dipole which might screen the applied bias. Similarly, when electrons (or holes) overcame the FET threshold voltage, internal field can be reduced due to the screening effect from the injected charges. Note that ambipolar transport materials are hardly being biased into full depletion condition, where signal can be easily justified and assigned to EA. In this case, there is always injection of either carriers (holes or electrons), which might contribute to the non-zero 2ω in-phase (Fig. S5(a)) signal. A contribution of quadrature phase signal in the 1ω signal (Fig. S5(d)) might be owed to the non-linear response of some long lived species[1] with respect to the gate modulation frequency. These render difficult to accurately predict the signal dependence, both in in-phase and quadrature phase at electrode edge (Fig. S5).

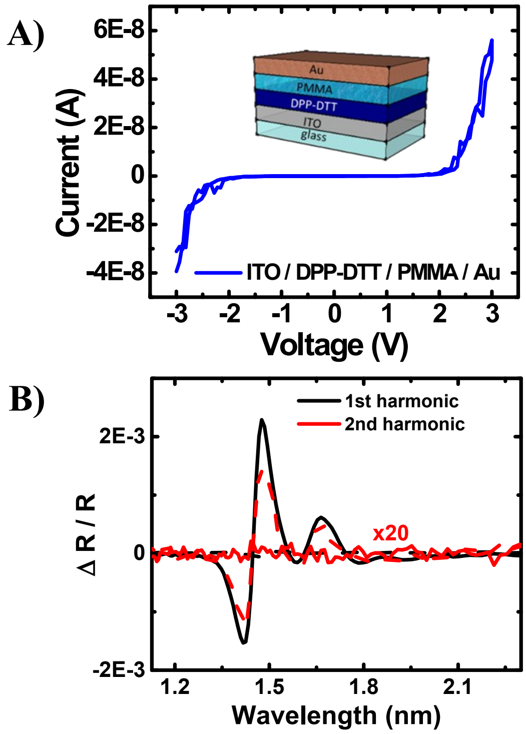

Figure S6. Electro-absorption measurement of DPPT-TT diode**.** (a, b) Current-voltage characteristics (a) and electro-absorption (b) reflectance measurement of the DPPT-TT MIS diode. In-phase and quadrature phase signals are shown with continuous and dashed lines, respectively. The device configuration is shown in the inset of (a). The spectra were collected by applying 1 V ± 0.25 V to Au, while ITO (indium tin oxide) is grounded (similar spectra are obtained when reversing the bias polarity to the diode).

When acquiring the EA signal of the DPPT-TT MIS diode, care has been taken to ensure that the total voltage (a constant bias value V_{DC} with a superimposed sinusoidal stimulus V_{AC}) applied to DPPT-TT diode would fall within the non-current-injection range, *i.e.* from -1.5 V to 1.5 V (see current-voltage measurement of the DPPT-TT diode, Fig. S6(a)). In these conditions, only the EA is measured, since the acquired signals are solely contributed from the field dependence of the ground state optical transitions, as evidenced by the lack of the quadrature phase signal in both the 1ω and 2ω spectra (dashed lines Fig. S6(b)).

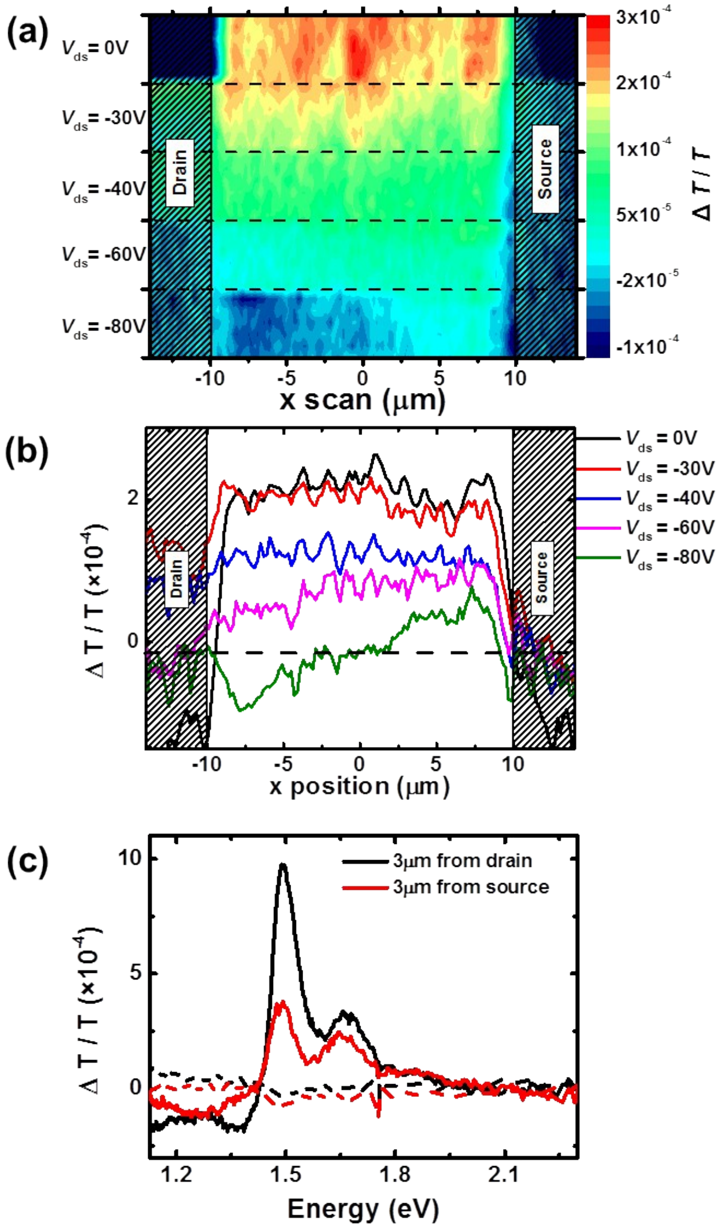

Figure S7. Charge carrier distribution for *h*-accumulation working regimes. (a) Charge modulation mapping of an FET operating in *h*-accumulation mode (V_{gs} = - 50 V ± 20 V) at different V_{ds} as indicated. The width of each map is 1.2μm. (b) Charge modulation line profiles detected along the channel and acquired under *h*-accumulation bias condition (V_{gs} = -50 V ± 20 V) at different V_{ds}. (c) Local spectra acquired within the active channel at ~ 3 μm away from drain (black) and source (right) electrode edges, with V_{gs} = - 50 V ± 20 V and V_{ds} = - 80 V. In-phase and quadrature phase signals are denoted with continuous and dashed lines, respectively.

Fig. S7 shows the charge carrier mapping performed in *h*-accumulation mode (Fig. S7(a) and Fig. S7(b)). An even distribution of charge carriers is recorded when V_{ds} is low (0 V to - 30 V). In this case, differently from the *e*-accumulation regime, a significant drop of carrier density occurs when drain-source is biased at V_{ds} < - 40 V. Such an effect has to be related to a much higher sensitivity of the device in *h*-accumulation mode to gate bias stress, producing a threshold voltage shift during measurements (lasting for 40 minutes to acquire a single map of 150 pixels (x scan) × 6 pixels (y scan) and a corresponding drop in the density of modulated carriers at the same modulating voltage). Such gate bias stress is evident in the output curves in *h*-accumulation, which show a reducing current for lower V_{ds} (Figure 1b). We mitigated the effect by selecting a higher absolute value for V_{gs} during the mapping (V_{gs} = - 50 V for holes and 30 V for electrons) and by alternating the acquisition of the maps in between *e*- and *h*- accumulation modes to detrap holes accumulated during long gate bias stressing. We tentatively attribute the higher instability to gate bias stress in *h*-accumulation to the presence of PEI, which is effective in promoting electrons injection, and besides partially reducing holes injection it could act as a source of holes trap states. Nevertheless, this effect does not prevent us from mapping the carriers distribution at lower V_{ds} values and to verify a correct switching from a unipolar to an ambipolar regime also in this case. In fact, at V_{ds} < - 60 V, the holes signal at the source does not evolve substantially, while it gradually decreases along the channel towards the drain as the device is entering saturation regime. For even lower V_{ds}, (V_{ds} = - 80 V), the charge-induced signal changes sign close to the drain electrode, as electrons are accumulated and the device enters the ambipolar regime.

Local spectra collected at ~ 3 μm away from either source or drain electrode under ambipolar injection regime (Fig. S7(c)) slightly deviate from CMS spectra acquired in the channel center (Fig. 2(b)). In particular we observe that intensity of spectrum acquired next to the source electrode (hole injection) is weaker than at the drain electrode (electron injection), which might be due to the bias stress of the device. The bias stress also affects electron injection, as the spectrum collected next to drain electrodes displays a mild contribution from EA signal. This brings to the experimental evidence that in the presence of significant contact resistance the potential drop does not occur only next to the electrode but rather it extends far within the channel. The mapping nevertheless is not affected, since we use a probing energy of 1.13 eV, where the signal is not substantially affected by EA. In this region where only charge absorption occurs, the change in the sign of the detected charge modulation signal is uniquely due to the presence of an opposite sign of the absorbing charges.

Electro-absorption

According to the perturbation theory, an EA spectrum is given by a linear combination of the absorption spectrum with all orders of field perturbation. Therefore, the main contributions to the spectra come from the first and second order of field dependence.[4, 5] Under non-injecting bias condition, the EA signal response shall experimentally follow the simplified equation:

$$\Delta\frac{T}{T}(\lambda) = \chi(\lambda)[\frac{F_{AC}^2}{2}(1+\cos(2\omega t)) + 2F_{AC}F_{DC}\cos(\omega t) + F_{DC}^2] \quad (1)$$

Where λ is the wavelength, χ is the electric susceptibility tensor, F_{AC} and F_{DC} are the alternating (AC) and direct (DC) component of the electric field, respectively, ω is the modulation angular frequency 2π*f* (*f* is modulation frequency), and *t* is time. This means that the signal acquired in the first harmonic (1ω) will be proportional to both the AC and DC component of electric field, while the signal acquired at the second harmonic (2ω) will only be proportional to the square of the AC component.

References List

1. C. Sciascia, M. Celebrano, M. Binda, D. Natali, G. Lanzani and J. R. Cabanillas-Gonzalez, *Org. Electron.*, 2012, **13**, 66-70.
2. D. Natali and M. Caironi, *Adv. Mater.*, 2012, **24**, 1357-1387.
3. C. Sciascia, N. Martino, T. Schuettfort, B. Watts, G. Grancini, M. R. Antognazza, M. Zavelani-Rossi, C. R. McNeill and M. Caironi, *Adv. Mater.*, 2011, **23**, 5086-5090.
4. P. J. Brown, H. Sirringhaus, M. Harrison, M. Shkunov and R. H. Friend, *Phys. Rev. B*, 2001, **63**, 125204.
5. A. Horvath, G. Weiser, G. Baker and S. Etemad, *Phys. Rev. B*, 1995, **51**, 2751.